JACS
JOURNAL OF THE AMERICAN CHEMICAL SOCIETY
Article
pubs.acs.org/JACS

High Thermoelectric Figure of Merit Values of Germanium Antimony Tellurides with Kinetically Stable Cobalt Germanide Precipitates

Felix Fahrnbauer, Daniel Souchay, Gerald Wagner, and Oliver Oeckler*

Institute for Mineralogy, Crystallography and Materials Science, Leipzig University, Scharnhorststraße 20, 04275 Leipzig, Germany

Supporting Information

ABSTRACT: Heterostructures that consist of a germanium antimony telluride matrix and cobalt germanide precipitates can be obtained by straightforward solid-state synthesis including simple annealing and quenching procedures. The microscale precipitates are homogeneously distributed in a matrix with pronounced "herringbone-like" nanostructure associated with very low thermal conductivities. In comparison to the corresponding pure tellurides, the figure of merit (ZT) values of heterostructured materials are remarkably higher. This is mostly due to an increase of the Seebeck coefficient with only little impact on the electrical conductivity. In addition, the phononic part of the thermal conductivity is significantly reduced in some of the materials. As a result, ZT values of ca. 1.9 at 450 °C are achieved. Temperature-dependent changes of the thermoelectric properties are well-understood and correlate with complex phase transitions of the telluride matrix. However, the high ZT values are retained in multiple measurement cycles.

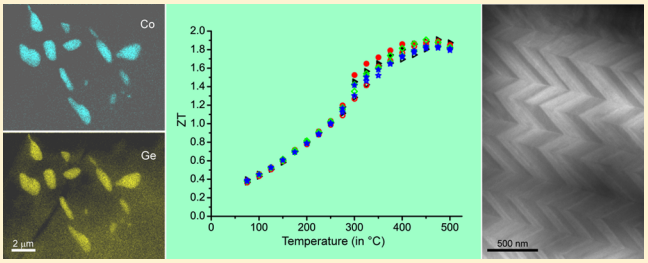

1. INTRODUCTION

The efficient use of waste heat is one of the great challenges toward economical energy consumption. Thermoelectric materials can directly convert heat to electricity and can thus contribute to solving the energy problem.[1,2] The efficiency of a thermoelectric generator depends on the average of its components' thermoelectric figure of merit (ZT) values, where $ZT = S^2\sigma T\kappa^{-1}$ and S = Seebeck coefficient, σ = electrical conductivity, and κ = thermal conductivity.[3] The optimization of one single property without influencing another is hardly possible, as S, σ, and the electronic part of the thermal conductivity κ_{el}, are interdependent. Transport properties depend on the band structure and, in part as a consequence, on the concentration and mobility of charge carriers.[4] Low charge carrier mobilities (μ) mean high Seebeck coefficients in combination with low electrical conductivities and vice versa. High Hall charge carrier concentrations n_H, on the other hand, result in high electrical conductivities and, according to the Wiedemann–Franz law $\kappa\sigma^{-1} = LT$ (with the Lorenz number L[5] as a proportionality constant), in high thermal conductivities.[6] Among the relevant properties, the phononic part of the thermal conductivity κ_{ph} can be almost independently influenced, e.g., by real-structure effects, such as point defects or domain boundaries. For example, SrTe nanoinclusions in PbTe form endotactically intergrown heterostructures, which after mechanical treatment reach ZT ≈ 2.2 at 640 °C.[7] Many heterostructures were synthesized as multilayer films, which enables well-defined crystalline samples but lacks the possibility of upscaling.[8−10] "Top-down" syntheses of nanostructured bulk material, on the other hand, include mechanical processing and sintering.[11,12] The large-scale synthesis of compact heterostructured materials more often relies on facile "bottom-up" approaches, e.g. by exsolution of minority phases upon quenching melts. This was found, for instance, in LAST (Pb–Sb–Ag–Te) materials, which exhibit nanoscale inclusions with coherent or semicoherent interfaces in a PbTe-rich matrix,[13,14] or in $AgSbTe_2$, which is in fact nonstoichiometric and includes Ag_2Te precipitates.[15,16] The control of composition and crystal structures of the phases in such materials is a challenge concerning efficient bulk syntheses.

Germanium antimony tellurides (GST materials) are discussed as thermoelectric materials.[17−21] Many of the compounds in the system $(GeTe)_nSb_2Te_3$ exhibit a rock salt-type high-temperature (HT) modification, which can be quenched to a metastable pseudocubic one. Such phases show planar defects parallel to {111}, which were found to drastically decrease the thermal conductivity, possibly by hindering long-wavelength phonon propagation.[20,22] Under ambient conditions, stable, long periodically ordered, layered phases consist of rock salt-type slabs separated by van der Waals gaps. At large GeTe fractions n, GST materials can be considered as doped variants of GeTe and are in line with several high ZT values of doped and alloyed GeTe materials.[23−27]

Te-containing cobalt gemanides were reported as possible thermoelectric materials due to a high n-type thermopower as well as a reasonable electrical conductivity.[28,29] Yet, cobalt germanides are not widely investigated as thermoelectric materials. They adopt various modifications, among which

Received: July 27, 2015
Published: September 15, 2015

DOI: 10.1021/jacs.5b07856
J. Am. Chem. Soc. 2015, 137, 12633−12638

$CoGe_2$ and Co_5Ge_7 were discussed as contact materials for $Si_{1-x}Ge_x$ technologies, mainly due to their high electrical conductivity.[30,31]

Thus, a combination of GST materials with intrinsic nanostructures and cobalt germanides as additional precipitates is an intriguing approach toward new thermoelectric composite materials.

2. EXPERIMENTAL SECTION

Synthesis. Compact ingots were obtained in silica glass ampules under dry Ar atmosphere by quenching stoichiometric melts of the pure elements Co (99.995%, Sigma-Aldrich), Sb (99.9999%, Smart Elements), Ge (99.999%, Smart Elements), and Te (puriss., VEB Spurenmetalle Freiberg) after 7−12 h at 950 °C. The samples were subsequently annealed at 590 °C for 1 d, again followed by quenching in water. Detailed information on the thermal treatment of the individual samples is given in the Supporting Information (Table S1). Plane-parallel samples for thermal conductivity measurements were obtained by using flat-bottomed silica glass ampules, splitting the ingots, and polishing specimens with SiC grinding powder. For resistivity and Seebeck coefficient measurements, cuboid slabs of the same ingots were sawn using a diamond wire saw.

Analytical Methods. Scanning electron microscopy (SEM) imaging and energy-dispersive X-ray spectroscopy (EDX) were done on a Zeiss LEO 1530 microscope (acceleration voltage 20 kV) equipped with an EDX detector (INCA system, Oxford Instruments). For room-temperature powder X-ray diffraction (PXRD) patterns of crushed samples on flat specimen holders, a Huber G670 diffractometer (Guinier geometry with imaging-plate detector and integrated read-out system) with Cu $K\alpha_1$ radiation [Ge(111) monochromator, λ = 1.540 51 Å] was used. Temperature-dependent measurements of samples in rotating silica glass capillaries under dry Ar atmosphere were recorded on a similar device with Mo $K\alpha_1$ radiation (λ = 0.710 73 Å) equipped with a ceramic heating fork for direct heat transfer.

Differential scanning calorimetry (DSC) of the powdered sample in an aluminum crucible was performed under He atmosphere [1 bar at room temperature (rt)] on a Q1000 DSC instrument (TA Instruments). The samples were heated at a rate of 10 K/min, held at the final temperature for 10 min, and subsequently cooled back to rt at 10 K/min. Two consecutive runs were performed.

Selected-area electron diffraction (SAED) and scanning transmission electron microscopy (STEM) imaging were done on a Philips CM-200 STEM (LaB_6 cathode, 200 kV, supertwin lens) with an R-TEM 136-5 EDX detector (EDAX) on dimpled and Ar ion-thinned (Duo-Mill, GATAN) samples.

Thermal diffusivity measurements were performed under He atmosphere with a Linseis LFA1000 apparatus equipped with an InSb detector. Simultaneous heat loss and finite pulse corrections were corrected using Dusza's model.[32] Values were averaged from five measurement points at each temperature. For κ calculation, they were multiplied with the Dulong−Petit heat capacity and the density as derived by the weight and the volume determined by Archimedes' principle. All densities were higher than 99% of the X-ray densities of the matrix material. The single values of each sample are given in Table S1 of the Supporting Information. S and σ were measured simultaneously under He atmosphere with a Linseis LSR-3 instrument with NiCr/Ni and Ni contacts and a continuous reverse of the polarity of the thermocouples (bipolar setup). Each transport property was measured on specimens cut from the ingots along different directions for comparison. No significant anisotropy was observed; obviously, all quenched samples were polycrystalline with randomly oriented grains. The errors of S and σ are smaller than 10%; for κ, they are ca. 5%. As a result, the ZT values given exhibit an absolute uncertainty of ca. 20%.[33] All measurements are well-reproducible and typical (not the very best) measurements are shown.

Computer programs and databases as well as their references are listed in section I of the Supporting Information.

3. RESULTS AND DISCUSSION

Structures and Composition. In order to demonstrate the influence of cobalt germanide precipitates on the thermoelectric properties of GST materials, this contribution focuses on three different GeTe contents described by n in the formula $(GeTe)_nSb_2Te_3$ (n = 12, 17, and 19). Preliminary experiments with various contents of cobalt germanide precipitates showed that the most promising thermoelectric properties are obtained for amounts around 1 wt %. Therefore, each pure GST phase is compared with samples that contain 1 wt % of $CoGe_2$ (corresponding to the nominal composition from starting materials). The simple procedure of quenching stoichiometric melts followed by annealing at 590 °C for 1 d yields precipitates of 1−2 μm in size that are homogeneously distributed in the GST matrix (cf. Figure 1). According to SEM images using backscattered electrons (BSE), the precipitate distribution does not change during heating and cooling cycles, e.g. in thermoelectric measurements (cf. Figure S2 in the Supporting Information).

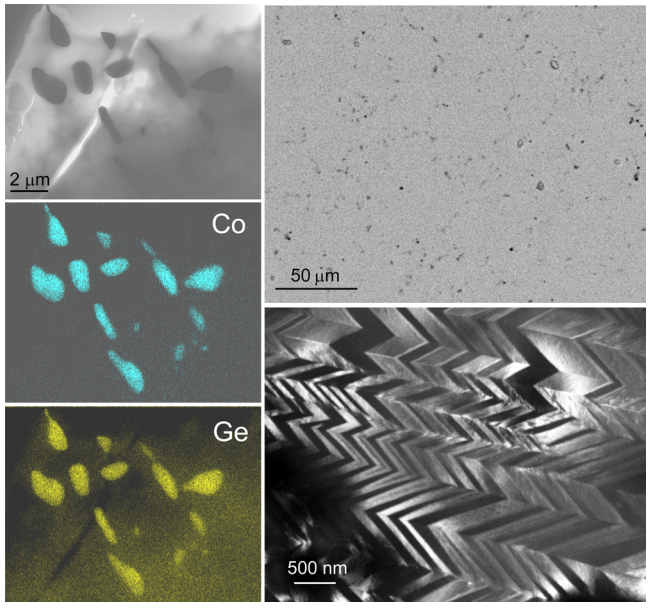

Figure 1. STEM-EDX element mapping of a sample with the nominal composition $(CoGe_2)_{0.2}(GeTe)_{17}Sb_2Te_3$ (left): bright-field image (top left) and spatially resolved element distribution for Co and Ge (middle and bottom, respectively). SEM-BSE image of a polished sample (top right) and STEM dark-field image of matrix region (bottom right, "herringbone-like structure", contrast due to orientation differences between neighboring domains and twinning).

SAED tilt series and EDX in a transmission electron microscope (TEM) reveal that the precipitates adopt the Co_5Ge_7 structure ($I4mm$,[34] a = 7.6 Å, c = 5.8 Å; cf. Figures S3 and S4 and Table S2 in the Supporting Information). Due to their very low overall fraction, the precipitates are hardly detectable by means of PXRD; only their strongest reflection corresponds to a tiny peak (cf. Figure S1 in the Supporting Information). The idealized stoichiometry of the precipitates slightly deviates from the nominal composition. According to TEM-EDX, however, the Co:Ge ratio in the precipitates varies, and the incorporation of small amounts of Te seems likely. In combination with a certain homogeneity range of GST,[21] this flexibility enables slight variations of the sample composition without the precipitation of further side phases.

DOI: 10.1021/jacs.5b07856
J. Am. Chem. Soc. 2015, 137, 12633−12638

In good agreement with literature reports, $(GeTe)_{12}Sb_2Te_3$ is pseudocubic after quenching,[35] whereas $(GeTe)_{17}Sb_2Te_3$ and $(GeTe)_{19}Sb_2Te_3$ exhibit average structures that are disordered variants of the rhombohedral α-GeTe type.[36] This results in strongly broadened and split reflections, as shown in the PXRD patterns given in Figure S1 in the Supporting Information. PXRD data are probably not sufficient to decide whether extended van der Waals gaps are present, as the corresponding structures may be almost homometric.[37] Quenched $(GeTe)_{17}Sb_2Te_3$ exhibits a pronounced, "herringbone-like" nanostructure (see Figure 1), both in samples with and without precipitates. Comparable nanostructures discussed in the literature for GST material with low Sb content and GeTe itself correlate with very low thermal conductivities.[20,22] After the first heating above 250 °C and slow cooling, all matrix phases adopt an average α-GeTe-type structure (for PXRD patterns of quenched vs slowly heated and cooled samples, see Figure S2 in Supporting Information). Upon thermal cycling, no changes of the matrix composition are observed (see Table S2 in Supporting Information). Within the detection limits of EDX, no Co is incorporated in the matrix.

Thermoelectric Properties and Phase Changes. The physical properties of GST materials depend on the thermal treatment as a consequence of their well-understood phase transitions.[17,20] Since an irreversible phase change from the metastable pseudocubic to the trigonal layered modification occurs around 240 °C for quenched $(GeTe)_{12}Sb_2Te_3$ (and, although less pronounced, also for the other samples), all samples were cycled three times to 240 °C in order to verify the kinetic stability in this temperature region [cf. Figure S5 in the Supporting Information for corresponding measurements for $(CoGe_2)_{0.2}(GeTe)_{17}Sb_2Te_3$]. Once the samples are heated beyond 250 °C, the irreversible phase transition yields different curves at lower temperatures, which do not change in all further cycles. Figure 2 correlates structural changes during the first heating of $(CoGe_2)_{0.2}(GeTe)_{17}Sb_2Te_3$ to higher temperatures with abrupt changes in the Seebeck coefficient and thermal conductivity. As the precipitates are not detectable by means of PXRD, the following discussion focuses on structural changes in the GST matrix material only.

Temperature T1 (~240 °C) marks the transition from the metastable pseudocubic to the trigonal layered modification in the heating curve (cf. left part of Figure 2) and is also visible in the property measurement curves (end of the almost linear increase of S). At T2 (~330 °C), the transition from the trigonal to the rock salt-type HT modification is visible, which is reversible upon cooling (T3, ~260 °C). Note that the pseudocubic modification does not recur once the sample was heated beyond ~240 °C. Therefore, all following cycles only show the transition between the trigonal and the rock salt-type modification. This reversible process is diffusion-controlled and thus exhibits a slight hysteresis that can also be seen in the thermoelectric property measurements. This hysteresis is also evident from differential scanning calorimetry (Figure 2), which yields more precise transition temperatures than temperature-dependent PXRD. However, DSC lacks the crucial information on the structural changes from the metastable to the stable phase that are associated with very small enthalpy values and produce a very broad signal around 200 °C that can hardly be distinguished from the baseline. Slight shifts of the temperatures when comparing thermoelectric property measurements and DSC with temperature-dependent PXRD might be due to a slower phase transition of the bulk sample during thermoelectric measurements compared to the powders heated for PXRD and to certain coarsening required to produce detectable X-ray reflections. The DSC maxima correspond to the beginning of changes in the PXRD patterns.

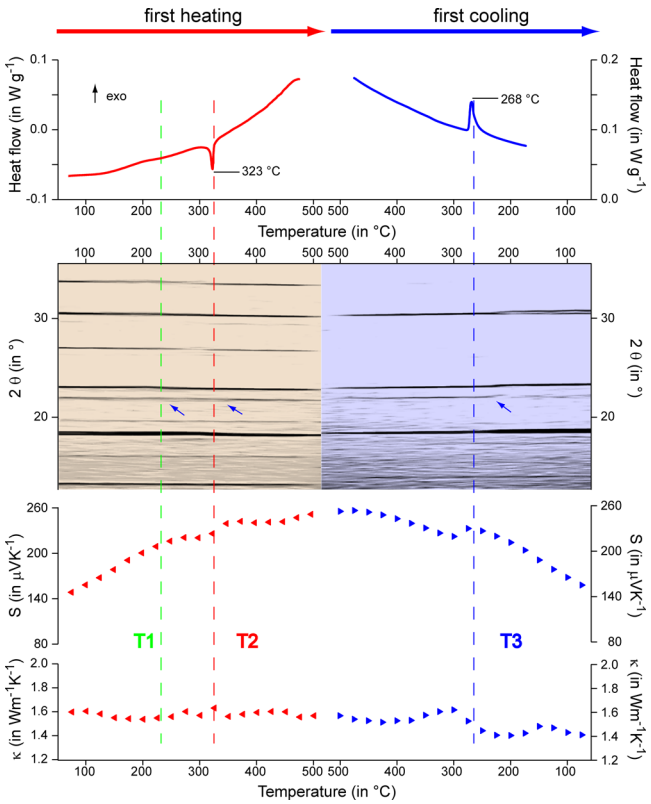

Figure 2. Thermal behavior of a sample with the nominal composition $(CoGe_2)_{0.2}(GeTe)_{17}Sb_2Te_3$: DSC measurements (top panel), temperature-dependent PXRD (second panel; note that the ordinate represents 2θ and the abscissa is the temperature), first heating cycle of Seebeck coefficient S (third panel), and thermal conductivity κ (bottom panel) measurements. Red symbols correspond to heating and blue symbols to cooling measurements. T1 (green), T2 (blue), and T3 (red) (see the text) are indicated as dashed lines. Changes in reflections, e.g., splitting as indicative of phase transitions, are marked by blue arrows; note that missing reflections upon cooling are due to single-crystalline material after melting.

The influence of the irreversible phase transition on the properties is most pronounced for $(GeTe)_{12}Sb_2Te_3$, less pronounced for $(GeTe)_{17}Sb_2Te_3$, and absent for $(GeTe)_{19}Sb_2Te_3$ (which already exhibits the trigonal structure after quenching). Comparable changes have also been reported for GST materials doped with In, Sn, and Se.[18,35,39] The differences between the first heating beyond 250 °C and consecutive curves are not reflected by the ZT curve. In order to eliminate the influence of the metastable pseudocubic GST modification for the sake of focusing on long-term stable states, the following discussion is based on the second heating cycle between room temperature and 500 °C (i.e., the second heating beyond 250 °C). For a combined plot of all cycles for each property for the $(CoGe_2)_{0.2}(GeTe)_{17}Sb_2Te_3$ sample, see Figures S5 and S6 in the Supporting Information.

For all examined GST materials with varying GeTe contents, the Seebeck coefficients are in the same range and show comparable temperature dependencies (see Figure 3). Higher values are obtained in heterostructured samples. They are observed over the whole temperature range for

DOI: 10.1021/jacs.5b07856
J. Am. Chem. Soc. 2015, 137, 12633−12638

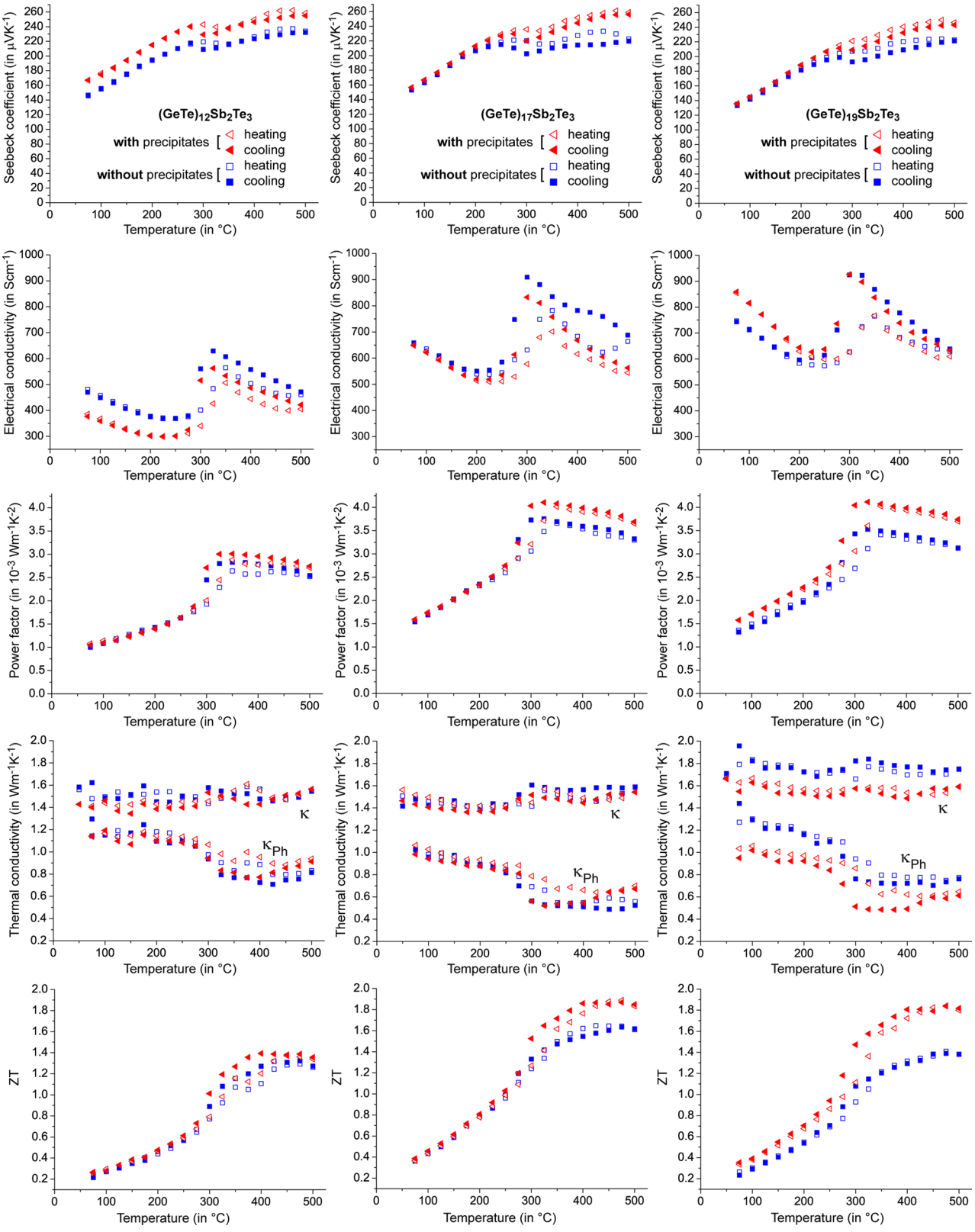

Figure 3. Thermoelectric properties of $(GeTe)_{12}Sb_2Te_3$ vs $(CoGe_2)_{0.15}(GeTe)_{12}Sb_2Te_3$ (left column), $(GeTe)_{17}Sb_2Te_3$ vs $(CoGe_2)_{0.2}(GeTe)_{17}Sb_2Te_3$ (middle column), and $(GeTe)_{19}Sb_2Te_3$ vs $(CoGe_2)_{0.22}(GeTe)_{19}Sb_2Te_3$ (right column); values for pure GST material are given as squares, and those for the corresponding heterostructured materials are given as triangles; empty symbols correspond to heating, filled ones correspond to cooling curves. Seebeck coefficient (first row), electrical conductivity (second row), power factor (third row), thermal conductivity and phononic part of thermal conductivity calculated from the thermal conductivity using a Lorenz number of 2.00×10^{-8} W Ω K^{-2} (which is a typical value for GST materials[38]) (fourth row), and ZT values (fifth row).

DOI: 10.1021/jacs.5b07856
J. Am. Chem. Soc. 2015, 137, 12633−12638

$(CoGe_2)_{0.15}(GeTe)_{12}Sb_2Te_3$ and at elevated temperatures within the existence range of the rock salt-type GST modification for $(CoGe_2)_{0.2}(GeTe)_{17}Sb_2Te_3$ and $(CoGe_2)_{0.22}(GeTe)_{19}Sb_2Te_3$, respectively. As a trend, samples with higher GeTe contents are better electrical conductors than those containing less GeTe. In heterostructured samples, the electrical conductivities are in the same range as those of the respective pure compounds. Within the existence range of the layered GST modification, σ is lower in heterostructured $(CoGe_2)_{0.15}(GeTe)_{12}Sb_2Te_3$ compared to $(GeTe)_{12}Sb_2Te_3$, while there is no influence in the $(CoGe_2)_{0.2}(GeTe)_{17}Sb_2Te_3$ sample and there is an increase for $(CoGe_2)_{0.22}(GeTe)_{19}Sb_2Te_3$ compared to the corresponding GST compounds. At elevated temperatures, both $(GeTe)_{12}Sb_2Te_3$ and $(GeTe)_{17}Sb_2Te_3$ exhibit slightly higher σ than the heterostructured samples, and there is no difference between $(GeTe)_{19}Sb_2Te_3$ and $(CoGe_2)_{0.22}(GeTe)_{19}Sb_2Te_3$.

These results are reflected in the power factor $S^2\sigma$, which is improved in all heterostructured samples at elevated temperatures. This effect is most pronounced for $(CoGe_2)_{0.22}(GeTe)_{19}Sb_2Te_3$, where both S and σ are increased.

As discussed in previous works, measurements of the heat capacity of several GST materials[18,20] yielded values close to those obtained with the Dulong−Petit approximation, especially when the reliability range of the single measurements is taken into account.[38] In the present cases, this approximation thus introduces errors of only a few percent. There is no significant difference in the thermal conductivities between heterostructured and pure $(GeTe)_nSb_2Te_3$ with n = 12 and 17 (cf. Figure 3). For n = 19, a significant decrease upon heterostructuring is achieved. Because the electrical conductivity is higher at the same time, the phononic contribution to the thermal conductivity is significantly lower in heterostructured $(CoGe_2)_{0.22}(GeTe)_{19}Sb_2Te_3$ than in $(GeTe)_{19}Sb_2Te_3$.

The ZT values exhibit a plateau above ∼400 °C (Figure 3). Therefore, is it reasonable to discuss the maximum values. An improvement of the ZT values upon heterostructuring is observed, which becomes more pronounced with increasing n. Not numerically significant for n = 12, it is very pronounced for $(CoGe_2)_{0.22}(GeTe)_{19}Sb_2Te_3$, whose ZT values are higher than those of $(GeTe)_{19}Sb_2Te_3$ over the whole measured temperature range and reach 0.9 at 250 °C and 1.8 at 450 °C. These improvements of up to 30% compared to the pure material are significant. All measurements and peak ZT values of up to 1.9 for $(CoGe_2)_{0.2}(GeTe)_{17}Sb_2Te_3$ are reproducible in at least four consecutive cycles (see Figure S5 in the Supporting Information).

4. CONCLUSION

Heterostructuring with cobalt germanides significantly enhances the thermoelectric properties of GST materials and yields samples with a remarkable kinetic stability concerning the amount, size, and distribution of precipitates. Samples can be easily synthesized by fusing the elements and simple annealing processes, in contrast to, e.g., syntheses that rely on time-consuming mechanical alloying and sintering procedures. The properties remain reproducible in many subsequent heating and cooling cycles, and the maximum ZT values do not decrease upon cycling. Most pronounced, the Seebeck coefficient is increased by the introduction of precipitates, which is most likely due to a decrease of the Hall carrier mobilities or their overall concentration and overcompensates occasionally lower electrical conductivities. The low overall fraction of precipitates does not change the microstructure of the matrix GST phase significantly, but still exhibits a pronounced influence on thermoelectric properties. The types and amounts of phases present do not change, except for the well-known reversible phase transitions of the GST matrices.

Further optimization might include other types of precipitates and a thorough optimization of the precipitate content in order to obtain optimum ZT values. Theoretical calculations based on the single parabolic band model may help to approach this in a targeted manner.[40] The possibly complex interplay between doping effects (both in the precipitates and in the matrix phase) and scattering at interfaces and domain boundaries remains a challenge for analytical methods.

■ ASSOCIATED CONTENT

Supporting Information

The Supporting Information is available free of charge on the ACS Publications website at DOI: 10.1021/jacs.5b07856.

Details on syntheses, powder X-ray diffraction, scanning and transmission electron microscopy, and thermoelectric measurements (PDF)

■ AUTHOR INFORMATION

Corresponding Author

*oliver.oeckler@gmx.de

Author Contributions

The manuscript was written through contributions of all authors.

Notes

The authors declare no competing financial interest.

■ ACKNOWLEDGMENTS

The work was funded by the European Union (European Social Fund, NFG "Effiziente Energienutzung: Neue Konzepte und Materialien") and the Deutsche Forschungsgemeinschaft (Grant OE530/1-2). We thank Christina Fraunhofer and Markus Nentwig for some syntheses and preliminary measurements, as well as Henry Auer, André Götze, and Prof. Dr. Holger Kohlmann for help with temperature-dependent PXRD and DSC measurements.

■ REFERENCES

(1) Zheng, X. F.; Liu, C. X.; Yan, Y. Y.; Wang, Q. *Renewable Sustainable Energy Rev.* **2014**, *32*, 486.

(2) Sootsman, J. R.; Chung, D. Y.; Kanatzidis, M. G. *Angew. Chem., Int. Ed.* **2009**, *48*, 8616.

(3) DiSalvo, F. J. *Science* **1999**, *285*, 703.

(4) Pei, Y.; Wang, H.; Snyder, G. J. *Adv. Mater.* **2012**, *24*, 6125.

(5) Kumar, G. S.; Prasad, G.; Pohl, R. O. *J. Mater. Sci.* **1993**, *28*, 4261.

(6) Franz, R.; Wiedemann, G. *Ann. Phys.* **1853**, *165*, 497.

(7) Biswas, K.; He, J.; Blum, I. D.; Wu, C.-I; Hogan, T. P.; Seidman, D. N.; Dravid, V. P.; Kanatzidis, M. G. *Nature* **2012**, *489*, 414.

(8) Zide, J.; Vashaee, D.; Bian, Z.; Zeng, G.; Bowers, J.; Shakouri, A.; Gossard, A. *Phys. Rev. B: Condens. Matter Mater. Phys.* **2006**, *74*, 205335.

(9) Kim, S. I.; Ahn, K.; Yeon, D.-H.; Hwang, S.; Kim, H.-S.; Lee, S. M.; Lee, K. H. *Appl. Phys. Express* **2011**, *4*, 091801.

(10) Zhang, Y.; Stucky, G. D. *Chem. Mater.* **2014**, *26*, 837.

(11) Joshi, G.; Lee, H.; Lan, Y.; Wang, X.; Zhu, G.; Wang, D.; Gould, R. W.; Cuff, D. C.; Tang, M. Y.; Dresselhaus, M. S.; Chen, G.; Ren, Z. *Nano Lett.* **2008**, *8*, 4670.

DOI: 10.1021/jacs.5b07856
J. Am. Chem. Soc. 2015, 137, 12633−12638

(12) Xie, W.; He, J.; Kang, H. J.; Tang, X.; Zhu, S.; Laver, M.; Wang, S.; Copley, J. R. D.; Brown, C. M.; Zhang, Q.; Tritt, T. M. *Nano Lett.* **2010**, *10*, 3283.
(13) Hsu, K. F.; Loo, S.; Guo, F.; Chen, W.; Dyck, J. S.; Uher, C.; Hogan, T.; Polychroniadis, E. K.; Kanatzidis, M. G. *Science* **2004**, *35*, 818.
(14) Androulakis, J.; Hsu, K. F.; Pcionek, R.; Kong, H.; Uher, C.; D'Angelo, J. J.; Downey, A.; Hogan, T.; Kanatzidis, M. G. *Adv. Mater.* **2006**, *18*, 1170.
(15) Armstrong, R. W.; Faust, J. W.; Tiller, W. A. *J. Appl. Phys.* **1960**, *31*, 1954.
(16) Wang, H.; Li, J.-F.; Zou, M.; Sui, T. *Appl. Phys. Lett.* **2008**, *93*, 202106.
(17) Schneider, M. N.; Rosenthal, T.; Stiewe, C.; Oeckler, O. *Z. Kristallogr.* **2010**, *225*, 463.
(18) Rosenthal, T.; Urban, P.; Nimmrich, K.; Schenk, L.; de Boor, J.; Stiewe, C.; Oeckler, O. *Chem. Mater.* **2014**, *26*, 2567.
(19) Yan, F.; Zhu, T. J.; Zhao, X. B.; Dong, S. R. *Appl. Phys. A: Mater. Sci. Process.* **2007**, *88*, 425.
(20) Rosenthal, T.; Schneider, M. N.; Stiewe, C.; Döblinger, M.; Oeckler, O. *Chem. Mater.* **2011**, *23*, 4349.
(21) Sankar, R.; Wong, D. P.; Chi, C.-S.; Chien, W.-L.; Hwang, J.-S.; Chou, F.-C.; Chen, L.-C.; Chen, K.-H. *CrystEngComm* **2015**, *17*, 3440.
(22) Lee, H. S.; Kim, B.-S.; Cho, C.-W.; Oh, M.-W.; Min, B.-K.; Park, S.-D.; Lee, H.-W. *Acta Mater.* **2015**, *91*, 83.
(23) Gelbstein, Y.; Davidow, J.; Girard, S. N.; Chung, D. Y.; Kanatzidis, M. G. *Adv. Energy Mater.* **2013**, *3*, 815.
(24) Wu, D.; Zhao, L.-D.; Hao, S.; Jiang, Q.; Zheng, F.; Doak, J. W.; Wu, H.; Chi, H.; Gelbstein, Y.; Uher, C.; Wolverton, C.; Kanatzidis, M. G.; He, J. *J. Am. Chem. Soc.* **2014**, *136*, 11412.
(25) Davidow, J.; Gelbstein, Y. *J. Electron. Mater.* **2013**, *42*, 1542.
(26) Zhu, T.; Gao, H.; Chen, Y.; Zhao, X. *J. Mater. Chem. A* **2014**, *2*, 3251.
(27) Schröder, T.; Rosenthal, T.; Giesbrecht, N.; Maier, S.; Scheidt, E.-W.; Scherer, W.; Snyder, G. J.; Schnick, W.; Oeckler, O. *J. Mater. Chem. A* **2014**, *2*, 6384.
(28) Vaqueiro, P.; Sobany, G. G.; Guinet, F.; Leyva-Bailen, P. *Solid State Sci.* **2009**, *11*, 1077.
(29) Laufek, F.; Navrátil, J.; Plášil, J.; Plecháček, T. *J. Alloys Compd.* **2008**, *460*, 155.
(30) Sun, H. P.; Chen, Y. B.; Pan, X. Q.; Chi, D. Z.; Nath, R.; Foo, Y. L. *Appl. Phys. Lett.* **2005**, *86*, 071904.
(31) Choi, J.; Lim, D. K.; Kim, Y.; Kim, S. *J. Phys. Chem. C* **2010**, *114*, 8992.
(32) Dusza, L. *High Temp. - High Pressures* **1995/1996**, *27/28*, 467.
(33) Pei, Y.; Shi, X.; LaLonde, A.; Wang, H.; Chen, L.; Snyder, G. J. *Nature* **2011**, *473*, 66.
(34) Schubert, K.; Anantharaman, T. R.; Ata, H. O. K.; Meissner, H. G.; Pötzschke, M.; Rossteutscher, W.; Stolz, E. *Naturwissenschaften* **1960**, *47*, 512.
(35) Rosenthal, T.; Welzmiller, S.; Oeckler, O. *Solid State Sci.* **2013**, *25*, 118.
(36) Schneider, M. N.; Urban, P.; Leineweber, A.; Döblinger, M.; Oeckler, O. *Phys. Rev. B: Condens. Matter Mater. Phys.* **2010**, *81*, 184102.
(37) Schneider, M. N.; Seibald, M.; Lagally, P.; Oeckler, O. *J. Appl. Crystallogr.* **2010**, *43*, 1012.
(38) Fahrnbauer, F.; Maier, S.; Grundei, M.; Giesbrecht, N.; Nentwig, M.; Rosenthal, T.; Wagner, G.; Snyder, G. J.; Oeckler, O. *J. Mater. Chem. C* **2015**, in press (DOI: 10.1039/C5TC01509J).
(39) Rosenthal, T.; Neudert, L.; Ganter, P.; de Boor, J.; Stiewe, C.; Oeckler, O. *J. Solid State Chem.* **2014**, *215*, 231.
(40) Pei, Y.; Wang, H.; Snyder, G. J. *Adv. Mater.* **2012**, *24*, 6125.

DOI: 10.1021/jacs.5b07856
J. Am. Chem. Soc. 2015, 137, 12633−12638